Neural-Network Computation Using Spin-Wave-Coupled Spin-Torque Oscillators

Hiroko Arai and Hiroshi Imamura

Phys. Rev. Applied **10**, 024040 — Published 27 August 2018

DOI: 10.1103/PhysRevApplied.10.024040

Neural network computation using spin-wave coupled spin torque oscillators

Hiroko Arai*
National Institute of Advanced Industrial Science and Technology (AIST), Spintronics Research Center, Tsukuba, Ibaraki, 305-8568, Japan and JST PRESTO, Kawaguchi, Saitama, 332-0012, Japan

Hiroshi Imamura†
National Institute of Advanced Industrial Science and Technology (AIST), Spintronics Research Center, Tsukuba, Ibaraki, 305-8568, Japan

A neural network computation scheme is proposed based on perceptron model having processing units which consist of spin-wave coupled spin-torque-oscillators. This is an oscillatory neural network, where the relative phase of the oscillators is controlled by tuning the Dzylaoshinshkii-Moriya interaction and applying oscillating magnetic filed. Each processing unit receives input signal which is an oscillating magnetic field and transmits alternating current. The alternating current is a function of the relative phase and generates oscillating magnetic (Oersted) field around the wire where the current flows through. The generated Oersted field then becomes an input signal to the next processing unit. Solving the Landau-Lifshitz-Gilbert equation, we obtain an activation function of the processing unit. Finally, an artificial neural network is constructed using the obtained activation function to recognize the handwritten digits in the MNIST database.

I. INTRODUCTION

Artificial neural network (ANN) is a neuromorphic computational construct designed to mimic the neural network in the brain [1]. Recently, much attention has been focused on information processing using ANNs, such as for object detection and recognition [2, 3], and in other business fields [4]. Because of the rapid progress of the machine power of the computers in operation speed, memory capacity, etc., software applications using ANN have come close to meet the performance in practical usage. However, energy consumption of computers is much larger than that of the brain.

Software applications are typically developed on central processing unit (CPU) or graphics processing unit (GPU) of computer machines, which are so-called von Neumann architecture. In order to further improve the performance of the ANN including energy consumption, building non-von Neumann architecture is intriguing and considerably attractive [5]. Neuromorphic architecture has adopted TrueNorth chip which is fabricated by complementary metal-oxide-semiconductors (CMOS) technology [2]. Not only the conventional devices in CMOS technology [2, 6], but also the new functional devices are candidates of elements for ANN such as atomic switch [7], memristor [8–11], coupled phase oscillator [12, 13], and spintronics devices [14–25].

Spintronics devices are easily fabricated on CMOS devices because the technology to manufacture spintronics devices is similar to that of manufacturing CMOS devices, which is a great advantage in developing ANN operating with CPU. Also they can typically be fabricated in nano-size scale, which is another advantage to reduce the spatial dimension of ANN system as a whole. Among various spintronics devices, spin torque oscillator (STO) is one of the suitable candidates for ANN. This is because neurons in the brain shows periodic spiking behavior, and STO was found to essentially have the same oscillation property with a biological neuron [26]. The STOs provide additional advantages. For example, the GHz band precession of the STOs provides high speed operation. Also, thermal tolerances and radiation resistance will be beneficial for easing the limit of operation condition in various environment. So far neuromorphic applications using the STO operating principle are reported such as associative memories [18–20], pattern matching [22–24], and spoken-digit recognition [25]. Most of these studies were performed by focusing on the synchronization property, i.e., whether STOs are locked, or not. In other words, the artificial neuron is implicitly assumed to possess the activation function of a step function. However, artificial neurons in software applications of ANN allow other activation functions such as the sigmoid function and the rectified linear unit (ReLU) function [3]. Because the performance of ANN can be improved by using these non-linear functions. It is therefore interesting to construct an artificial neuron which incorporates STO having the activation function with other shapes of step functions.

In this paper, a neural network computation scheme using a spin-wave coupled spin-torque-oscillator is proposed. Especially, the basic concept and working principles are brought into focus. The activation function of the processing unit is obtained by solving the Landau-Lifshitz-Gilbert equation. Then the ANN using the obtained activation function is constructed to recognize the handwritten digits in the MNIST database [27].

* arai-h@aist.go.jp
† h-imamura@aist.go.jp

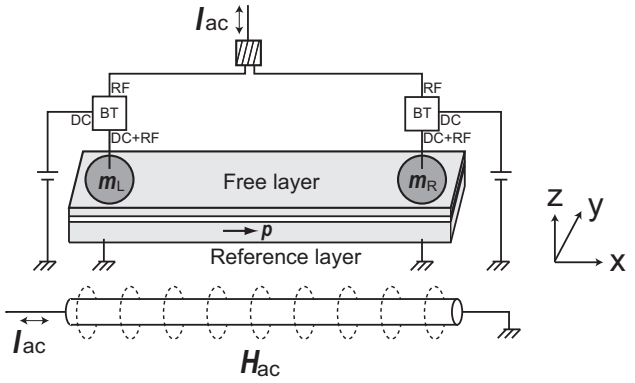

FIG. 1. Schematic illustration of the processing unit consisting of a spin-wave coupled STOs. The magnetization directions of the free layers of the left and the right STOs are represented by the unit vectors $\boldsymbol{m}_{\rm L}$ and $\boldsymbol{m}_{\rm R}$, respectively. The direct current is applied to the STOs through each point contact. The oscillating magnetic field, $\boldsymbol{H}_{\rm ac}$, generated by the alternating current is also applied. The alternating current, $I_{\rm ac}$, which is the sum of the AC from the bias tees (BTs) at each point contact, generates the oscillating magnetic (Oersted) field, $\boldsymbol{H}_{\rm Oe}$, around the wire where the current flows through as indicated by the dotted circles. The generated Oersted field becomes an input signal to the next processing unit. The Cartesian coordinates are also shown. The direction of the magnetization of the reference layer, $\boldsymbol{p}$, is fixed to the positive x-direction.

II. RESULTS AND DISCUSSION

A. Single unit

Figure 1 shows a schematic illustration of the processing unit consisting of a spin-wave coupled STOs, which is a laterally-long magnetic resistant device with double point contacts. The magnetization directions of the free layers of the left and the right STOs are represented by the unit vectors $\boldsymbol{m}_{\rm L}$ and $\boldsymbol{m}_{\rm R}$, respectively. The direct current is applied to the STOs through each point contact to induce the oscillation dynamics of magnetizations underneath the point contacts, the dynamics of which are coupled with each other by spin waves in the free layer. The coupling is assumed to comprise the Heisenberg interaction (HI) and the Dzyaloshinskii-Moriya interaction (DMI). The HI prefers the collinear magnetic structure on one hand, and the DMI prefers the non-colinear magnetic structure on the other hand. Tuning the ratio of the strength of the DMI to that of the HI, one can control the relative phase of the oscillations of $\boldsymbol{m}_{\rm L}$ and $\boldsymbol{m}_{\rm R}$.

Summing up the alternating current from the bias tees (BTs) at each point contact by a combiner, we obtain the total alternating current, $I_{\rm ac}$, which is a function of the relative phase. This comes from the fact that the oscillating component of the resistance of each STO is inversely proportional to the inner product $\boldsymbol{m}_{\rm L(R)}\cdot\boldsymbol{p}$, where $\boldsymbol{p}$ is the direction of the magnetization in the reference layer. The amplitude of $I_{\rm ac}$ for the in-phase oscillation is larger than that of the out-of-phase oscillation. The relative phase can also be controlled by applying oscillating magnetic field which exerts a torque on $\boldsymbol{m}_{\rm L}$ and $\boldsymbol{m}_{\rm R}$ to result in the in-phase oscillation. If the spatial separation of the STOs and the strength of the DMI are designed such that the out-of-phase oscillation is induced at $H_{\rm ac}=0$, the output signal, $I_{\rm ac}$, increases with the increase of the input signal, $H_{\rm ac}$. The output signal of the processing unit is the oscillating magnetic (Oersted) field generated around the wire where $I_{\rm ac}$ flows through. The function representing the relation between the input and output signals of the processing unit is called activation function, which plays an important role in ANNs.

The activation function of the spin-wave coupled STOs is obtained by solving the Landau-Lifshitz-Gilbert equation having the Sloczewski spin torque term under oscillating magnetic field,

$$\frac{d\boldsymbol{m}}{dt} = -\gamma(\boldsymbol{m}\times\boldsymbol{H}_{\rm eff}) + v\boldsymbol{m}\times(\boldsymbol{m}\times\boldsymbol{p}) + \alpha\left(\boldsymbol{m}\times\frac{d\boldsymbol{m}}{dt}\right), \tag{1}$$

where γ is the gyromagnetic ratio, and α is the Gilbert damping constant. Here $\boldsymbol{m}=\boldsymbol{m}(\boldsymbol{r},t)$ represents the magnetization unit vector at position $\boldsymbol{r}$ and at time t. The arguments $\boldsymbol{r}$ and t are omitted for convenience. The effective field $\boldsymbol{H}_{\rm eff}$ is given by the sum of the HI field, the DMI field, and the oscillating external magnetic field. The HI field is given by,

$$\boldsymbol{H}_{\rm HI} = \frac{2A}{\mu_0 M_{\rm s}}\nabla^2\boldsymbol{m}, \tag{2}$$

where A is the stiffness constant, μ_0 is the magnetic permeability of vacuum, and $M_{\rm s}$ is the saturation magnetization. The DMI field is given by,

$$\boldsymbol{H}_{\rm DMI} = \frac{2D}{\mu_0 M_{\rm s}}\left(\frac{\partial m_z}{\partial x},\frac{\partial m_z}{\partial y},-\frac{\partial m_x}{\partial x}-\frac{\partial m_y}{\partial y}\right), \tag{3}$$

where D is the DMI constant which ranges from 0.05 to 1.0 mJ/m^2 depending on the materials [28]. Throughout this paper we assume that the free layer is designed in such away that the magnetic anisotropy field cancels with the demagnetization field. The oscillating external magnetic field is given by

$$\boldsymbol{H}_{\rm ac} = H_{\rm ac}\sin(2\pi f t)\boldsymbol{e}_y, \tag{4}$$

where $\boldsymbol{e}_y$ is the unit vector pointing in the positive y-direction, and f is the oscillation frequency. The second term in the right-hand side in Eq. (1) represents the spin-torque term, where $\boldsymbol{p}$ is fixed to the positive x-direction, $\boldsymbol{p}=(1,0,0)$. The coefficient v is defined as

$$v = \frac{g\,\mu_{\rm B}\,J\,P}{2|e|M_{\rm s}d(1+P^2\boldsymbol{m}\cdot\boldsymbol{p})}, \tag{5}$$

where g is the Landé g-factor of the electron spin, $\mu_{\rm B}$ is the Bohr magneton, J is current density through a

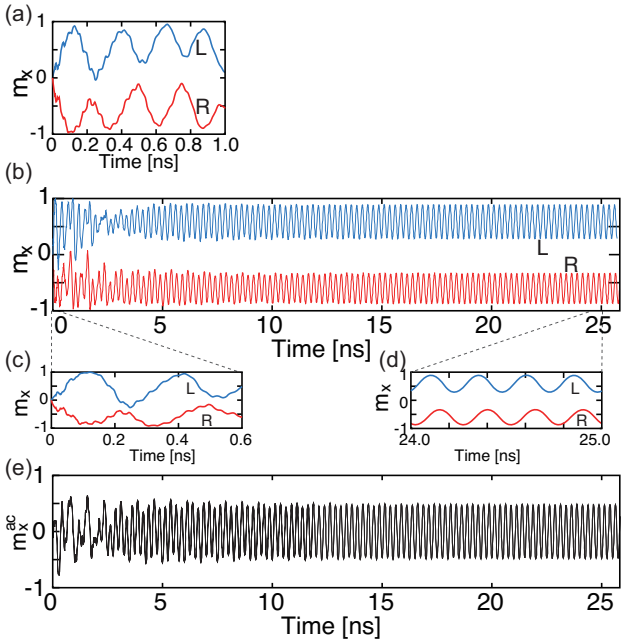

FIG. 2. (a) The time evolution of the x-component of $\boldsymbol{m}_{\rm L}$ and $\boldsymbol{m}_R$ at $H_{\rm ac} = 0$ are plotted by the blue and red curves, respectively. (b) The same plot at $H_{\rm ac} = 300$ (Oe). (c) Enlarged view of (b) for $t = 0 - 0.6$ (nsec). (d) Enlarged view of (b) for $t = 24 - 25$ (nsec). (e) The time evolution of $m_x^{\rm ac}$ for $H_{\rm ac} = 300$ (Oe).

region of the point contact, P is the spin polarization, e is electron charge, and d is the thickness of the free layer.

The shape of the free layer is assumed as 2 nm wide, 40 nm long, and 1 nm thick. The free layer is modeled by an one-dimensional magnetization chain and is divided into the cells with the size of $2 \times 2 \times 1$ (nm^3). The simulations are performed by using mumax^3 code [29]. The STOs are represented by the cells at the left and right ends, $\boldsymbol{m}_{\rm L}$ and $\boldsymbol{m}_{\rm R}$, where the direct bias current is applied. The positive current is defined as the electrons flowing from the free layer to the reference layer.

The material parameters for the free layer are assumed as follows: $M_{\rm s} = 8 \times 10^5$ (A/m), $P = 0.5$, $\alpha = 0.01$, $A = 7 \times 10^{-12}$ (J/m), and $D = 8 \times 10^{-4}$ (J/m^2). The density of the direct bias current is $J = 6 \times 10^{11}$ (A/m^2), and the initial state is $\boldsymbol{m} = (0, 0, 1)$ for all calculations.

B. Activation function

The processing unit is carefully designed to show an anti-phase oscillation at $H_{\rm ac} = 0$ as mentioned earlier. The specific result is shown in Fig. 2(a), where the blue and red curves represent the x-component of $\boldsymbol{m}_{\rm L}$ and $\boldsymbol{m}_{\rm R}$ as a function of time, respectively. An application of oscillating magnetic field drastically changes the relative phase of $\boldsymbol{m}_{\rm L}$ and $\boldsymbol{m}_{\rm R}$. Figure 2(b) shows the results under the oscillating magnetic field, $H_{\rm ac} = 300$ (Oe) with

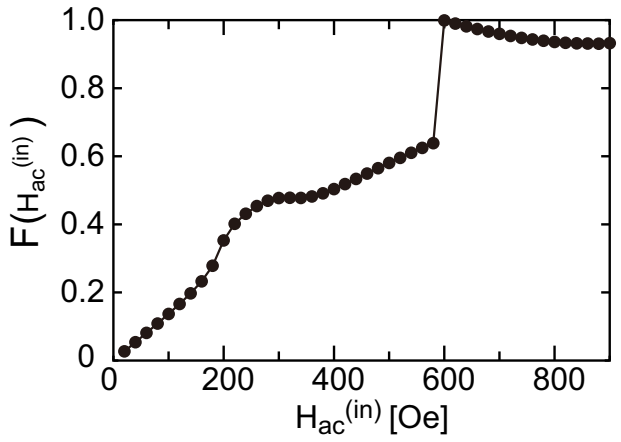

FIG. 3. The value of the activation function F obtained at each $H_{\rm ac}$.

$f = 4$ (GHz) which is the oscillation frequency at $H_{\rm ac} = 0$. The initial anti-phase oscillation shown in Fig. 2(c) becomes nearly in-phase after a few nano seconds and the in-phase oscillation is stabilized even after 25 nano seconds as shown in Fig. 2(d).

The oscillating and non-oscillating components of the current from the STOs are first separated by the bias-tee. Then the oscillating components are summed up by a combiner (hatched box) to produce $I_{\rm ac}$ as shown in Fig. 1. The alternating current $I_{\rm ac}$, and therefore the magnetic field $H_{\rm ac}$ generated by $I_{\rm ac}$ are proportional to the sum of the oscillating components of $\boldsymbol{m}_{\rm L}$ and $\boldsymbol{m}_{\rm R}$, which is denoted by $m_x^{\rm ac}$ and is shown in Fig. 2(e).

Let us introduce the activation function F defined as

$$H_{\rm ac}^{(\rm out)} = c\, F\left[H_{\rm ac}^{(\rm in)}\right], \tag{6}$$

where $H_{\rm ac}^{(\rm in)}$ is the external oscillating magnetic field applied to the processing unit, and $H_{\rm ac}^{(\rm out)}$ is the oscillating magnetic field generated by the processing unit. The coefficient c is a constant, the value of which is determined so that the activation function ranges from 0 to 1. The F value at each $H_{\rm ac}^{(\rm in)}$ is obtained by analyzing $m_x^{\rm ac}$ as shown in Fig. 3, where the amplitude of $m_x^{\rm ac}$ is averaged for $t = 40 - 50$ (nsec). It increases with the increase of $H_{\rm ac}^{(\rm in)}$ below 600 Oe because the precession cone angle increases with the increase of $H_{\rm ac}^{(\rm in)}$. It shows a hump at around 300 Oe because the mode of spin wave changes. It also shows a jump at $H_{\rm ac}^{(\rm in)} = 600$ (Oe) above which $\boldsymbol{m}_{\rm R}$ precesses with $m_z < 0$.

C. Artificial neural network

Since the activation function obtained shown in Fig. 3 indicates a shifted-sigmoid-like function, one can expect that the spin wave-coupled STOs work as nodes of an

ANN. We constructed an ANN using the obtained activation function to recognize the handwritten digits in the MNIST database [27]. As shown in Fig. 4(a), the ANN consists of three layers: the input layer, the hidden layer, and the output layer. The input layer has 784 nodes, receiving input signals from normalized gray-scaled pictures with 28×28 pixels. The hidden layer has 50 nodes. The output layer has 10 nodes, corresponding to the numbers from 0 to 9 digits.

We briefly noted the hardware implementation of the weights. As mentioned above, the input and output signals are the oscillating magnetic field, so that the weights should modify the amplitude and the phase if the weight is negative. These operations can be performed by using a device such as an analog multiplier. In addition, the product-sum operations between the output signals from nodes and weights are performed as superposition of the waves. However, in this study, we simply performed the product-sum operations by summing the values as mentioned below.

Introducing the variable $x_{\rm orig}^{(i)}$ ranging from 0 to 1 to represent the gray scale of the i-th pixel, the input signal of the i-th processing unit is set as $H_{{\rm ac},i}^{({\rm in})} = 900 x_{\rm orig}^{(i)}$. From Eq. (6), the input-output relation of the i-th processing unit is given by

$$H_{{\rm ac},i}^{({\rm out})} = c\, F\left[H_{{\rm ac},i}^{({\rm in})}\right], \tag{7}$$

where the coefficient c is set as 90 Oe. The output signal from the STO in the input layer is multiplied by the value of weight $\boldsymbol{W}_1$. The input signal to the node j in the hidden layer is given by

$$H_{{\rm ac},j}^{({\rm in})} = \sum_{i=1}^{784} H_{{\rm ac},i}^{({\rm out})} W_{1,ij}, \tag{8}$$

where $W_{1,ij}$ is the weight.

The output signal from the j-th node in the hidden layer is given by

$$H_{{\rm ac},j}^{({\rm out})} = c\, F\left[H_{{\rm ac},j}^{({\rm in})}\right]. \tag{9}$$

Likewise, the input signal to the k-th node in the output layer is given by

$$H_{{\rm ac},k}^{({\rm in})} = \sum_{j=1}^{50} H_{{\rm ac},j}^{({\rm out})} W_{2,jk}, \tag{10}$$

where $\boldsymbol{W}_2$ is the weight between the hidden and output layers. Finally, the output signal from the k-th node in the output layer is obtained as

$$H_{{\rm ac},k}^{({\rm out})} = c\, F\left[H_{{\rm ac},k}^{({\rm in})}\right]. \tag{11}$$

The node with the largest value indicates the digit predicted by the ANN. A learning is to update the value of the weights to obtain an accurate prediction from ANN,

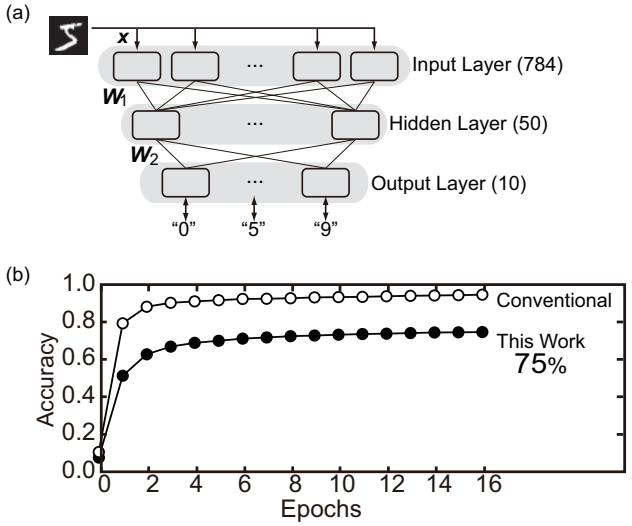

FIG. 4. (a) Schematic illustration of the ANN we constructed to recognize the handwriting digit in the MNIST database. Figures in brackets indicate the numbers of processing unit. The output signal from each layer is multiplied by the weight, $W_{1{\rm or}2}$, and then the total amount of the signals are fed to the next layer. (b) Transition of the accuracy for the recognition obtained from conventional neural network (open circles) and by this work (filled circles).

and is performed by the back propagation method. For simplicity, in the back propagation, we replace the activation function with the analytical sigmoid function as $F(x) = 1/\{1+\exp(-a(x-x_0))\}$ with a gain $a = 0.02$ and a shift $x_0 = 600$, which has a similar shape to that shown in Fig. 3. The cross-entropy error function was used for the estimation of error between the prediction by ANN and the correct answer given by the MNIST database. The 60,000 images were used for training (learning), and other 10,000 images were used for testing. Figure 4(b) shows the accuracy of the recognition as a function of epochs. The conventional ANN consists of nodes with activation function of the typical sigmoid function given by $F(x) = 1/\{1+\exp(x)\}$. The conventional ANN produces 95% accuracy on average from the same structure in Fig. 4(a). The accuracy of the STO-based ANN is 75%, which is smaller than that of the conventional ANN. We noted that the lower accuracy results from the shape of the activation function. One may consider that the reason of the lower accuracy is a disharmony of the shape between the activation functions for the forward and backward calculation during the training process. However, even when the shifted sigmoid function was used for both the forward and backward processes, the recognition accuracy remains around 75%. In order to increase the accuracy, one should rather tune the hyperparameters such as the number of nodes in hidden layer, the number of hidden layer, and learning rate.

III. CONCLUSIONS

In summary, neural network computation is proposed based on perceptron model having processing units which consist of spin-wave coupled spin-torque-oscillator. The activation function of the processing unit is obtained by solving the Landau-Lifshitz-Gilbert equation incorporating Slonczewski term. The artificial neural network is constructed using the activation function obtained from the study. The recognition of the handwritten digits in the MNIST database is demonstrated with the accuracy of 75%.

ACKNOWLEDGMENTS

We would like to thank Hiroyuki Akinaga, Shingo Tamaru, Hitoshi Kubota, and Takehiko Yorozu for valuable discussions. This work was supported by JST PRESTO (JPMJPR1421).

[1] D. Hassabis, D. Kumaran, C. Summerfield, and M. Botvinick, Neuroscience-Inspired Artificial Intelligence, Neuron **95**, 245 (2017).

[2] P. A. Merolla, J. V. Arthur, R. Alvarez-Icaza, A. S. Cassidy, J. Sawada, F. Akopyan, B. L. Jackson, N. Imam, C. Guo, Y. Nakamura, B. Brezzo, I. Vo, S. K. Esser, R. Appuswamy, B. Taba, A. Amir, M. D. Flickner, W. P. Risk, R. Manohar, and D. S. Modha, A million spiking-neuron integrated circuit with a scalable communication network and interface, Science **345**, 668 (2014).

[3] Y. LeCun, Y. Bengio, and G. Hinton, Deep learning, Nature **521**, 436 (2015).

[4] M. Tkac and R. Verner, Artificial neural networks in business: Two decades of research, Appl. Soft Comp. **38**, 788 (2016).

[5] C. D. Schuman, T. E. Potok, R. M. Patton, J. D. Birdwell, M. E. Dean, G. S. Rose, and J. S. Plank, A Survey of Neuromorphic Computing and Neural Networks in Hardware, arXiv: 1705.06963 (2017).

[6] P. Maffezzoni, B. Bahr, Z. Zhang, and L. Daniel, Oscillator Array Models for Associative Memory and Pattern Recognition, IEEE Trans. Circ. Sys. I: Regular Papers **62**, 1591 (2015).

[7] T. Hasegawa, K. Terabe, T. Tsuruoka, and M. Aono, Atomic Switch: Atom/Ion Movement Controlled Devices for Beyond Von-Neumann Computers, Adv. Mat. **24**, 252 (2012).

[8] S.-H. Jo, T. Chang, I. Ebong, B. B. Bhadviya, P. Mazumder, and W. Lu, Nanoscale Memristor Device as Synapse in Neuromorphic Systems, Nano Lett. **10**, 1297 (2010).

[9] T. Chang, S.-H. Jo, and W. Lu, Short-Term Memory to Long-Term Memory Transition in a Nanoscale Memristor, ACS Nano **5**, 7669 (2011).

[10] A. Chanthbouala, V. Garcia, R. O. Cherifi, K. Bouzehouane, S. Fusil, X. Moya, S. Xavier, H. Yamada, C. Deranlot, N. D. Mathur, M. Bibes, A. Barthélémy, and J. Grollier, A ferroelectric memristor, Nat. Mat. **11**, 860 (2012).

[11] M. Prezioso, F. Merrikh-Bayat, B. D. Hoskins, G. C. Adam, K. K. Likharev, and D. B. Strukov, Training and operation of an integrated neuromorphic network based on metal-oxide memristors, Nature **521**, 61 (2015).

[12] P. Kaluza, Computation with phase oscillators: An oscillatory perceptron model, Neurocomputing **118**, 127 (2013).

[13] M. J. Cotter, Y. Fang, S. P. Levitan, D. M. Chiarulli, and V. Narayanan, Computational Architectures Based on Coupled Oscillators, in 2014 IEEE Computer Society Annual Symposium on VLSI (2014) pp. 130–135.

[14] P. Krzysteczko, J. Münchenberger, M. Schäfers, G. Reiss, and A. Thomas, The Memristive Magnetic Tunnel Junction as a Nanoscopic Synapse-Neuron System, Adv. Mat. **24**, 762 (2012).

[15] A. Sengupta, S. H. Choday, Y. Kim, and K. Roy, Spin orbit torque based electronic neuron, Appl. Phys. Lett. **106**, 143701 (2015).

[16] G. Srinivasan, A. Sengupta, and K. Roy, Magnetic Tunnel Junction Based Long-Term Short-Term Stochastic Synapse for a Spiking Neural Network with On-Chip STDP Learning, Sci. Rep. **6**, 29545 (2016).

[17] C. M. Liyanagedera, A. Sengupta, A. Jaiswal, and K. Roy, Stochastic Spiking Neural Networks Enabled by Magnetic Tunnel Junctions: From Nontelegraphic to Telegraphic Switching Regimes, Phys. Rev. Appl. **8**, 064017 (2017).

[18] T. Shibata, R. Zhang, S. Levitan, D. Nikonov, and G. Bourianoff, CMOS supporting circuitries for nano-oscillator-based associative memories, in 13th International Workshop on Cellular Nanoscale Networks and their Applications (CNNA) (2012) pp. 1–5.

[19] S. P. Levitan, Y. Fang, D. H. Dash, T. Shibata, D. E. Nikonov, and G. I. Bourianoff, Non-Boolean associative architectures based on nano-oscillators, in 13th International Workshop on Cellular Nanoscale Networks and their Applications (2012) pp. 1–6.

[20] D. Fan, S. Maji, K. Yogendra, M. Sharad, and K. Roy, Injection-Locked Spin Hall-Induced Coupled-Oscillators for Energy Efficient Associative Computing, IEEE Trans. Nanotech. **14**, 1083 (2015).

[21] W. A. Borders, H. Akima, S. Fukami, S. Moriya, S. Kurihara, Y. Horio, S. Sato, and H. Ohno, Analogue spin–orbit torque device for artificial-neural-network-based associative memory operation, Appl. Phys. Express **10**, 013007 (2016).

[22] K. Yogendra, D. Fan, and K. Roy, Coupled Spin Torque Nano Oscillators for Low Power Neural Computation, IEEE Trans. Magn. **51**, 4003909 (2015).

[23] D. Nikonov, G. Csaba, W. Porod, T. Shibata, D. Voils, D. Hammerstrom, I. A. Young, and G. I. Bourianoff, Coupled-Oscillator Associative Memory Array Operation for Pattern Recognition, IEEE J. Explor. Solid-State Comp. Dev. Circ. **1**, 85 (2015).

[24] K. Kudo and T. Morie, Self-feedback electrically coupled spin-Hall oscillator array for pattern-matching operation, Appl. Phys. Express **10**, 043001 (2017).

[25] J. Torrejon, M. Riou, F. A. Araujo, S. Tsunegi, G. Khalsa, D. Querlioz, P. Bortolotti, V. Cros, K. Yakushiji, A. Fukushima, H. Kubota, S. Yuasa, M. D. Stiles, and J. Grollier, Neuromorphic computing with nanoscale spintronic oscillators, Nature **547**, 428 (2017).

[26] H. Arai and H. Imamura, Stochastic Phase Synchronization of Perpendicularly Magnetized Spin-Torque Oscillators with the Second-Order Uniaxial Anisotropy, IEEE Trans. Magn. **53**, 6100705 (2017).

[27] Y. Lecun, C. Cortes, and C. J. C. Burges, http://yann.lecun.com/exdb/mnist/.

[28] K. Nawaoka, S. Miwa, Y. Shiota, N. Mizuochi, and Y. Suzuki, Voltage induction of interfacial Dzyaloshinskii–Moriya interaction in Au/Fe/MgO artificial multilayer, Appl. Phys. Express **8**, 063004 (2015).

[29] A. Vansteenkiste, J. Leliaert, M. Dvornik, M. Helsen, F. Garcia-Sanchez, and B. V. Waeyenberge, The design and verification of MuMax3, AIP Advances **4**, 107133 (2014).